Eur. Phys. J. D (2017) 71: 160
DOI: 10.1140/epjd/e2017-70710-1

THE EUROPEAN PHYSICAL JOURNAL D

Regular Article

Electron-induced double ionization of oriented methane molecules*

Dahbia Oubaziz[1], Zakia Aitelhadjali[1], Michele Arcangelo Quinto[2], Rachida Boulifa[1], and Christophe Champion[3,a]

[1] Laboratoire de Génie Electrique, LGE, Université Mouloud Mammeri de Tizi-Ouzou, 15000 Tizi-Ouzou, Algeria
[2] Instituto de Física Rosario, CONICET, Universidad Nacional de Rosario, S20000EKF Rosario, Argentina
[3] Centre d'Etudes Nucléaires de Bordeaux Gradignan, CENBG, CNRS/IN2P3, Université de Bordeaux, 33170 Gradignan, France

Received 14 November 2016 / Received in final form 24 April 2017
Published online 15 June 2017 – © EDP Sciences, Società Italiana di Fisica, Springer-Verlag 2017

Abstract. We report here a theoretical study of the target orientation effect on the total cross sections for the double ionization of methane molecules impacted by electrons. The theoretical description is performed within the first Born approximation. The initial state of the collisional system is composed of an electron projectile modeled by a plane wave and a molecular target described by a one-center wave function while the final state is constituted by a scattered electron described by a plane wave and two ejected electrons both represented by a Coulomb wave and coupled with a Gamow factor. Secondary electron energetic distributions and total cross sections are reported for particular target configurations. Strong orientation effects on the double-ionization process are pointed out in particular when scrutinized *orbital by orbital*.

1 Introduction

Generally speaking, collision physics informs about the structure of matter at the atomic and molecular level with relevant applications in various areas of science and technology like plasma physics, planetary atmospheres [1–8] and radiobiology. Along past decades, an intensive effort of experimental and theoretical work has been devoted to the study of the single ionization of atoms and molecules induced by electron impact. On the contrary, the double ionization of atomic and molecular systems remains poorly documented. In this context, the rare existing studies on electron-induced double ionization of molecules are, to the best of our knowledge, essentially focused on the determination of *multiple differential* cross sections and therefore limited to simple molecules. In this context, let us cite the works of Chuluunbaatar et al. [9] and Mansouri et al. [10], both based on the plane-wave Born approximation model (PWBA) and focused on the description of the $(e, 3e)$ experiments of Lahmam Bennani et al. [11] on a H_2 target. However, in the second work - developed within the second Born approximation [10] – a strong disagreement with the experimental observations [11] was reported by the authors with, in particular, small shifts of the binary and recoil peaks [10]. Let us also cite the more recent experiment of Li et al. [12] where double ionization of neon, argon, and molecular nitrogen targets impacted by 600 to 700 eV electron beams was investigated. Thus, the fourfold differential cross sections obtained have demonstrated that the double ionization of small atoms or molecules was dominated - at least within the energy range studied (600–700 eV) – by non-first-order mechanisms such as the two-step (TS2) one, as previously shown by Staicu Casagrande et al. for helium [13] and methane [14].

Regarding the double ionization of oriented molecules, there are, to the best of our knowledge, only a few cases reported in the literature. Nevertheless, let us mention the photon- and ion-induced double ionization of molecular deuterium (D_2) [15] and that of H_2 impacted by photons [16]. For equal energy sharing between the two ejected electrons and the photon (∼76 eV), the authors observed a strong dependence of the electron angular distribution versus the orientation of the molecular target axis. This effect was well reproduced by a model in which a pair of photo-ionization amplitudes was introduced for the light polarization parallel to as well as perpendicular to the molecular axis. Finally, we have recently reported in references [17–20] a detailed study of the water and methane double ionization within the first Born approximation and reported a strong dependence of the fivefold differential cross sections with respect to the target molecular orientation.

On other hand, the case of photon-induced double ionization recently treated by Ivanov and Kheifets [21] who used the time dependent Schrödinger equation for calculating the total double-ionization cross sections of H_2. Besides, perpendicular to parallel photon-induced

* Contribution to the Topical Issue "Many Particle Spectroscopy of Atoms, Molecules, Clusters and Surfaces", edited by A.N. Grum-Grzhimailo, E.V. Gryzlova, Yu V. Popov, and A.V. Solov'yov.

[a] e-mail: champion@cenbg.in2p3.fr

double-ionization cross-section ratios were also reported by Vanroose et al. [22] and compared to their homologous cross-section ratios obtained by single photo-ionization. Thus, single-photo-ionization ratios exhibited peaks for photon energy of about 75 eV that corresponds to a Cooper-like minimum of the dipole in the parallel configuration. This maximum was also observed in the photon-induced double ionization cross-section ratios at slightly lower photon energy. Then, the authors stated that the perpendicular to parallel ratios were similar in both the single and double-ionization channels.

In the current paper we report a theoretical description of the double ionization of oriented methane molecules impacted by electrons. We briefly described hereafter the theoretical framework allowing the calculations of the total double ionization cross sections versus the molecular orientation. Then, we report the theoretical predictions in terms of total cross sections for secondary electrons ejected from the same molecular orbital, namely, the final states hereafter referred to as $1t_{2x}$, $1t_{2y}$, $1t_{2z}$, and $2a_1$.

2 Theoretical model

Only a brief summary of our theoretical approach is hereafter reported and for more details we refer the reader to our previous works [17–20].

In the first Born approximation, the fivefold differential ionization cross section (5DCS) is given by

$$\frac{d^5\sigma}{d\Omega_1 d\Omega_2 d\Omega_s dE_1 dE_2} \equiv \sigma^{(5)}(\Omega_1,\Omega_2,\Omega_s,E_1,E_2) = \sum_j^5 \sigma_j^{(5)}(\Omega_1,\Omega_2,\Omega_s,E_1,E_2) = (2\pi)^4 \frac{k_1 k_2 k_s}{k_i} \sum_j^5 |T_j|^2 \quad (1)$$

where $d\Omega_s$, $d\Omega_1$ and $d\Omega_2$ denote the solid angle elements of scattering and ejection while the energy intervals of the ejected electrons are represented by dE_1 and dE_2. The momenta of the incident, the scattered and the two ejected electrons are denoted by $\mathbf{k_i}$, $\mathbf{k}_s$, $\mathbf{k_1}$ and $\mathbf{k}_2$ respectively. In a $(e, 3e)$ reaction, the conservation of energy imposes $k_s = \sqrt{2(E_i - E_1 - E_2 - I^{2+})}$ where I^{2+} denotes the double ionization threshold. In this context, let us remark that in equation (1), the summation over the index j is limited to the five final states of the doubly ionized molecule, namely, those corresponding to the ejection of two electrons from the same molecular orbital.

The first Born term T_j is written as

$$T_j \equiv T_j(\alpha,\beta,\gamma) = \langle \Psi_f(\mathbf{k}_s,\mathbf{k}_1,\mathbf{k}_2,\mathbf{r}_0,\mathbf{r}_1,\mathbf{r}_2)|\, V(\mathbf{r}_0,\mathbf{r}_1,\mathbf{r}_2)| \times \Psi_i^j(\mathbf{k}_i,\mathbf{r}_0,\mathbf{r}_1,\mathbf{r}_2;\alpha,\beta,\gamma)\rangle \quad (2)$$

where $|\Psi_i^j(\mathbf{k}_i,\mathbf{r}_0;\mathbf{r}_1,\mathbf{r}_2;\alpha,\beta,\gamma)\rangle$ represents the initial state of the collisional system while $|\Psi_f(\mathbf{k}_s,\mathbf{k}_1,\mathbf{k}_2,\mathbf{r}_0;\mathbf{r}_1,\mathbf{r}_2)\rangle$ stands for the final state.

Let us add that we have here neglected the exchange effect between the secondaries and the scattered electron arguing that the latter is faster than any ejected one as reported hereafter when the limits of integration over the energy transfers are discussed to access to the total cross section. Besides, the exchange effect between the ejected electrons that may be very important in particular in symmetrical geometries, it is properly taken into account by discriminating the spin state of each particle in the final state.

The potential $V(\mathbf{r}_0,\mathbf{r}_1,\mathbf{r}_2)$ represents the Coulomb interaction between the incoming electron and the target and is written as

$$V = \frac{-6}{r_0} - \frac{1}{|\mathbf{r}_0-\mathbf{R}_1|} - \frac{1}{|\mathbf{r}_0-\mathbf{R}_2|} - \frac{1}{|\mathbf{r}_0-\mathbf{R}_3|} - \frac{1}{|\mathbf{r}_0-\mathbf{R}_4|} + \sum_{i=1}^{i=10} \frac{1}{|\mathbf{r}_0-\mathbf{r}_i|} \quad (3)$$

where $R_1 = R_2 = R_3 = R_4 = R_{CH} = 2.08$ a.u. [23] refers to the distance between the carbon atom and the hydrogen nuclei while $\mathbf{r}_0$ denotes the coordinate of the incident electron and $\mathbf{r}_i$ the position vector of the i^{th} bound electron with respect to the center of the molecule.

Furthermore, by using the frozen-core approximation the current 10-electron target problem may be reduced to a 2-electron one, that permits to express the initial state as $|\varphi(\mathbf{k}_i,\mathbf{r}_0)\varphi_i(\mathbf{r_1},\mathbf{r}_2;\alpha,\beta,\gamma)\rangle$ where $\varphi(\mathbf{k}_i,\mathbf{r}_o)$ refers to the plane wave function associated to the incident electron and $\phi_i(\mathbf{r}_1,\mathbf{r}_2;\alpha,\beta,\gamma)$ the single-center target wave function taken from reference [23], namely,

$$\varphi_i(\mathbf{r}_1,\mathbf{r}_2;\alpha,\beta,\gamma) = \upsilon_j(\mathbf{r}_1;\alpha,\beta,\gamma)\upsilon_j(\mathbf{r}_2;\alpha,\beta,\gamma), \quad (4)$$

with

$$\upsilon_j(\mathbf{r};\alpha,\beta,\gamma) = \sum_{k=1}^{N_{at}(j)} f_{jk}(r) \sum_{\mu=-l_{jk}}^{\mu=l_{jk}} \Delta_{\mu,m_{jk}}^{l_{jk}}(\alpha,\beta,\gamma) S_{l_{jk}}^{\mu}(\hat{r}). \quad (5)$$

The rotation matrix is defined by

$$\Delta_{\mu,m_{jk}}^{l_{jk}}(\alpha,\beta,\gamma) = e^{-m_{jk}\alpha} d_{\mu,m_{jk}}^{l_{jk}}(\beta) e^{-i\mu\gamma}, \quad (6)$$

where the quantity $d_{\mu,m_{jk}}^{l_{jk}}(\beta)$ is given by the Wigner formula

$$d_{\mu,m_{jk}}^{l_{jk}} = \sum_{t=0}^{\tau} (-1)^t \times \frac{\sqrt{(l_{jk}+\mu)!(l_{jk}-\mu)!(l_{jk}+m_{jk})!(l_{jk}-m_{jk})!}}{(l_{jk}+\mu-t)!(l_{jk}-m_{jk}-t)!t!(t-\mu+m_{jk})!} \times \xi^{2l_{jk}+\mu-m_{jk}-2t} \eta^{2t-\mu+m_{jk}}, \quad (7)$$

with $\xi = \cos(\beta/2)$, and $\eta = \sin(\beta/2)$.

The final state composed by a scattered electron and two ejected electrons is here described within the "2 Coulomb Wave-Gamow (2CWG)" model, namely,

$$\langle \Psi_f(\mathbf{k}_s,\mathbf{k}_1,\,\mathbf{k}_2,\,\mathbf{r}_0,\mathbf{r}_1,\mathbf{r}_2)| = \langle \varphi(\mathbf{k}_s,\mathbf{r}_0)\phi_f\,(\mathbf{k}_1,\mathbf{r}_1,\mathbf{k}_2,\mathbf{r}_2) \times \phi_G\,(|\mathbf{k_2}-\mathbf{k_1}|)\,| \quad (8)$$

where $\varphi(\mathbf{k}_s, \mathbf{r}_0)$ represents the plane wave function associated to the scattered electron while $\phi_f(\mathbf{k}_1, \mathbf{r}_1, \mathbf{k}_2, \mathbf{r}_2)$ refers to the Coulomb wave function introduced for describing each ejected electron. Finally, we also considered the electrostatic repulsion between the two outgoing electrons by introducing in equation (8) the Gamow factor $\phi_G(|\mathbf{k_2} - \mathbf{k_1}|)$ expressed as

$$\phi_G(|\mathbf{k_2} - \mathbf{k_1}|) = \exp\left(\frac{-\pi\chi_{12}}{2}\right)\Gamma(1 - i\chi_{12}), \quad (9)$$

with $\chi_{12} = \frac{1}{|\mathbf{k_2}-\mathbf{k_1}|}$.

Under these conditions and by using the well-known partial wave expansion of the plane waves as well as that of the Coulomb waves function, we get the following fivefold differential cross section (5DCS) corresponding to the jth orbital

$$\frac{d^5\sigma}{d\Omega_1 d\Omega_2 d\Omega_s dE_1 dE_2} = 2 \times (2\pi)^4 \frac{k_1 k_2 k_s}{k_i} \left(\phi_G(|\mathbf{k_2} - \mathbf{k_1}|)\right)^2 \times \sum_j^5 \left| T_j^{(1)}(\alpha,\beta,\gamma) + T_j^{(2)}(\alpha,\beta,\gamma) + T_j^{(3)}(\alpha,\beta,\gamma) \right|^2 \quad (10)$$

where

$$\begin{cases} T_j^{(1)}(\alpha,\beta,\gamma) = \Pi_j(\alpha,\beta,\gamma;\mathbf{k}_1)\,\hat{\Pi}_j(\alpha,\beta,\gamma;\mathbf{k}_2) \\ T_j^{(2)}(\alpha,\beta,\gamma) = \Pi_j(\alpha,\beta,\gamma;\mathbf{k}_2)\,\hat{\Pi}_j(\alpha,\beta,\gamma;\mathbf{k}_1) \\ T_j^{(3)}(\alpha,\beta,\gamma) = -\hat{\Pi}_j(\alpha,\beta,\gamma;\mathbf{k}_1)\,\hat{\Pi}_j(\alpha,\beta,\gamma;\mathbf{k}_2) \end{cases} \quad (11)$$

with

$$\prod_j(\alpha,\beta,\gamma;\mathbf{k}_1) = \frac{2}{qk_1}\sqrt{\frac{2}{\pi}} \sum_{k=1}^{N_{at}(j)} \sum_{l,m} \sum_{l_1,m_1} \times X_{jk}^{l,l_1}(k_1,q)\, i^{l-l_1} e^{i\sigma_{l_1}(\eta_1)} \times Y_{l_1}^{m_1}(\hat{k}_1)\, Y_l^{m*}(\hat{q})\, \Delta_{l_{jk},m_1-m,m_{jk}}(\alpha,\beta,\gamma) (-1)^{m_1}\sqrt{\frac{\hat{l}_1\hat{l}\hat{l}_{jk}}{4\pi}} \begin{pmatrix} l_1 & l & l_{jk} \\ 0 & 0 & 0 \end{pmatrix} \begin{pmatrix} l_1 & l & l_{jk} \\ -m_1 & m & m_1 - m \end{pmatrix} \quad (12)$$

with $\hat{l} = 2l + 1$, the momentum transfer defined by $\mathbf{q} = \mathbf{k}_i - \mathbf{k}_s$ and

$$\hat{\prod}_j(\alpha,\beta,\gamma;\mathbf{k}_1) = \frac{1}{\pi q k_1}\sqrt{\frac{2}{\pi}} \sum_{k=1}^{N_{at}(j)} \sum_{m_1=-l_{jk}}^{l_{jk}} \hat{X}_{jk}^{l_{jk}}(k_1)\, \Delta_{l_{jk},m_1,m_{jk}}(\alpha,\beta,\gamma)\, Y_{l_{jk}}^{m_1}(\hat{k})\, i^{-l_{jk}}\, e^{i\sigma_{l_{jk}}(\eta_1)} \quad (13)$$

where

See equation (14) next page.

The radial parts $X_{jk}^{l,l_1}(k,q)$ and $\hat{X}_{jk}^{l_{jk}}(k)$ introduced in equations (12) and (13) are expressed as

$$X_{jk}^{l,l_1}(k,q) = \int_0^\infty r\, F_{l_1}(k,r)\, j_l(qr)\, f_{jk}(r)\, dr \quad (15)$$

$$\hat{X}_{jk}^{l_{jk}}(k) = \int_0^\infty r\, F_{l_{jk}}(k,r)\, f_{jk}(r)\, dr \quad (16)$$

where $f_{jk}(r)$ refers to the jkth component of the radial part of the target (molecular) wave function while $F_l(kr)$ and $j_l(qr)$ denote the radial hypergeometric function and the Bessel function, respectively.

In equations (12) and (13), the quantity σ_l represents the Coulomb phase shift given by

$$\sigma_l(\eta) = \arg\Gamma(l + 1 + i\eta) = \arg\Gamma(l + 1 - 2i/k). \quad (17)$$

Besides, to benefit of the selectivity rules of the complex harmonics in the integrations over the ejection directions $\hat{k}_1$ and $\hat{k}_2$ and then to provide an analytical expression of the triply differential cross sections, we have here treated the electrostatic repulsion between the two outgoing electron by replacing the quantity $\left(\phi_G(|\mathbf{k_2} - \mathbf{k_1}|)\right)^2$ by the approximate Gamow factor $g_G(k_1,k_2)$ given by Defrance and co-workers [24,25], namely,

$$g_G(k_1,k_2) = \begin{cases} \frac{2\pi}{k_1}\dfrac{e^{-2\pi/k_1}}{1-e^{-2\pi/k_1}} & \text{when} \quad k_1 > k_2 \\ 0 \quad \text{when} \quad k_1 = k_2 \\ \frac{2\pi}{k_2}\dfrac{e^{-2\pi/k_2}}{1-e^{-2\pi/k_2}} & \text{when} \quad k_2 > k_1. \end{cases} \quad (18)$$

Then, the triply differential cross section (3DCS) may be written as

$$\frac{d^3\sigma(\alpha,\beta,\gamma)}{d\Omega_s dE_1 dE_2} = \iint \frac{d^5\sigma(\alpha,\beta,\gamma)}{d\Omega_1 d\Omega_2 d\Omega_s dE_1 dE_2} d\hat{k}_1 d\hat{k}_2 \quad (19)$$

where $d\hat{k} = \sin\theta\, d\theta\, d\phi$.

Finally, taking into account the closure relation of the spherical harmonics given by

$$\int Y_\ell^m(\hat{k}) Y_{\ell'}^{m'}(\hat{k}) d\hat{k} = \delta_{\ell\ell'}\delta_{mm'} \quad (20)$$

Equation (19) may be written as

$$\frac{d^3\sigma(\alpha,\beta,\gamma)}{d\Omega_s dE_1 dE_2} = 2(2\pi)^4 \frac{k_1 k_2 k_s}{k_i} g_G(k_1,k_2) \times \left\{ \sum_{j=1}^5 \Big[I_j(\alpha,\beta,\gamma;k_1)\hat{I}_j(k_2) + I_j(\alpha,\beta,\gamma;k_2)\hat{I}_j(k_1) + \hat{I}_j(k_1)\hat{I}_j(k_2) + 2Re(H_j(\alpha,\beta,\gamma;k_1)H_j^*(\alpha,\beta,\gamma;k_2)) - (2Re(H_j(\alpha,\beta,\gamma;k_1)\hat{I}_j(k_2)) + 2Re(H_j(\alpha,\beta,\gamma;k_2)\hat{I}_j(k_1)) \Big] \right\} \quad (21)$$

$$\Delta^{l_{jk}}_{\mu,m_{jk}}(\alpha,\beta,\gamma) = \left(\frac{D^{l_{jk}}_{\mu,-m_{jk}}(\alpha,\beta,\gamma) - D^{l_{jk}}_{\mu,m_{jk}}(\alpha,\beta,\gamma)}{\sqrt{2}}\right)\delta_{m_{jk},1}$$
$$+ i\left(\frac{D^{l_{jk}}_{\mu,-m_{jk}}(\alpha,\beta,\gamma) + D^{l_{jk}}_{\mu,m_{jk}}(\alpha,\beta,\gamma)}{\sqrt{2}}\right)\delta_{m_{jk},-1(-3)}(\text{for the } 1t_{2y} \text{ orbital})$$
$$\Delta^{l_{jk}}_{\mu,m_{jk}}(\alpha,\beta,\gamma) = \left(\frac{D^{l_{jk}}_{\mu,-m_{jk}}(\alpha,\beta,\gamma) - D^{l_{jk}}_{\mu,m_{jk}}(\alpha,\beta,\gamma)}{\sqrt{2}}\right)\delta_{m_{jk},1(3)}$$
$$+ i\left(\frac{D^{l_{jk}}_{\mu,-m_{jk}}(\alpha,\beta,\gamma) + D^{l_{jk}}_{\mu,m_{jk}}(\alpha,\beta,\gamma)}{\sqrt{2}}\right)\delta_{m_{jk},-1}(\text{for the } 1t_{2x} \text{ orbital})$$
$$\Delta^{l_{jk}}_{\mu,m_{jk}}(\alpha,\beta,\gamma) = i\left(\frac{D^{l_{jk}}_{\mu,m_{jk}}(\alpha,\beta,\gamma) - D^{l_{jk}}_{\mu,-m_{jk}}(\alpha,\beta,\gamma)}{\sqrt{2}}\right)\delta_{m_{jk},-2}$$
$$+ \left(D^{l_{jk}}_{\mu,m_{jk}}(\alpha,\beta,\gamma)\delta_{m_{jk},0}\right) \qquad \text{otherwise.} \tag{14}$$

where

$$I_j(\alpha,\beta,\gamma;k_1) = \frac{8}{\pi}\frac{1}{q^2k_1^2}\sum_{k=1}^{N_{at}(j)}\sum_{l,m}\sum_{l_1,m_1} X^{l,l_1}_{jk}(k_1,q)$$
$$\times i^l Y_l^{m*}(\hat{q})\Delta_{l_{jk},m_1-m,m_{jk}}(\alpha,\beta,\gamma)\sqrt{\frac{\hat{l}_1\hat{l}\hat{l}_{jk}}{4\pi}}$$
$$\times \begin{pmatrix} l_1\ l\ l_{jk} \\ 0\ 0\ 0 \end{pmatrix}\begin{pmatrix} l_1 & l & l_{jk} \\ -m_1 & m & m_1-m \end{pmatrix}$$
$$\times \sum_{\bar{k}'}^{N_{at}(j)}\sum_{l',m'} X^{l',l_1}_{jk'}(k_1,q) i^{-l'} Y_{l'}^{m'}(\hat{q})\Delta^*_{l_{jk'},m_1-m',m_{jk'}}(\alpha,\beta,\gamma)$$
$$\times \sqrt{\frac{\hat{l}_1\hat{l}'\hat{l}_{jk'}}{4\pi}}\begin{pmatrix} l_1\ l'\ l_{jk'} \\ 0\ 0\ 0 \end{pmatrix}\begin{pmatrix} l_1 & l' & l_{j\bar{k}'} \\ -m_1 & m' & m_1-m' \end{pmatrix} \tag{22}$$

$$H_j(\alpha,\beta,\gamma;k_1) = \frac{4}{\pi^2}\frac{1}{q^2k_1^2}\sum_{k=1}^{N_{at}(j)}\sum_{k'}^{N_{at}(j)}\sum_{l,m,m_1}$$
$$X^{l,l_{jk'}}_{jk}(k_1,q) i^l Y_l^{m*}(\hat{q})\hat{X}^{l_{jk'}}_{jk'}(k_1)\Delta_{l_{jk},m_1-m,m_{jk}}(\alpha,\beta,\gamma)$$
$$\times \Delta^*_{l_{jk'},m_1,m_{jk'}}(\alpha,\beta,\gamma)(-1)^{m_1}\sqrt{\frac{\hat{l}_{jk'}\hat{l}\hat{l}_{jk}}{4\pi}}\begin{pmatrix} l_{jk'}\ l\ l_{jk} \\ 0\ 0\ 0 \end{pmatrix}$$
$$\times \begin{pmatrix} l_{jk'} & l & l_{jk} \\ -m_1 & m & m_1-m \end{pmatrix} \tag{23}$$

and

$$\hat{I}_j(k_1) = \frac{2}{\pi^3}\frac{1}{q^2\,k_1^2}\sum_{k=1}^{N_{at}(j)}\left[\hat{X}^{l_{jk}}_{jk}(k_1)\right]^2. \tag{24}$$

In order to obtain the *total* (integrated) cross section (TCS), equation (21) is numerically integrated over the solid angle Ω_s and the ejected energies E_1 and E_2, namely

$$\sigma(\alpha,\beta,\gamma) = \int_0^{E_{1\,\max}}\int_0^{E_{2\,\max}}\int \frac{d^3\sigma(\alpha,\beta,\gamma)}{d\Omega_s\,dE_1\,dE_2}d\Omega_s\,dE_1\,dE_2. \tag{25}$$

Besides, the scattered electron being - by definition - the most energetic electron in the final state, we have followed the recommendations of Defrance et al. [24] and restricted the region of integration over the ejection energies E_1 and E_2 to $E_{1\,\max}$ and $E_{2\,\max}$ defined by

$$\begin{cases} E_{1\,\max} = (E_i - I^{2+})/2 \\ E_{2\,\max} = (E_i - I^{2+})/2 - E_1 \end{cases} \tag{26}$$

that is consistent with the spirit of the 1st Born approximation as highlighted by Bahati et al. [26].

In this context, let us add that, in order to justify the restriction of the upper limits of integration mentioned in equation (26), Defrance et al. have studied a variety of two-electron systems (He, Li^+, ..., N^{5+}) and reported that the region from $(E_i - I^{2+})/2$ to $(E_i - I^{2+})$ didn't contribute to the total cross section calculations appreciably [24].

3 Results and discussion

In the current work, we investigate the influence of the molecular target orientation on the total double ionization (DI) cross sections. To this end, we have selected particular orientations of the target methane molecule, namely, those deduced from the initial target orientation (α, β, γ) = (0,0,0) – which corresponds to a two hydrogen atoms of the CH_4 molecule are located in the yz plane (the two others being in the background) – by a β-angle rotation around the y axis (with β ranging from 0 to π) in keeping $\alpha = \gamma = 0$.

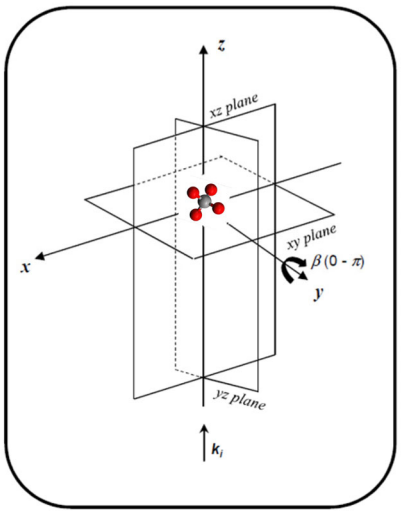

Fig. 1. Schematic representation of the particular rotations $R_y(0,\,\beta,\,0)$ investigated in the present work.

These different configurations will be hereafter denoted $R_y(0,\beta,0)$. Besides, let us note that in all the geometries investigated here, the incident momentum $\mathbf{k_i}$ remains collinear to the z axis (see Fig. 1).

Studying the orientation effects on the double ionization process for a single oriented methane molecule requires discriminating each molecular subshell contribution, the latter being dependent on the relative alignment of the impacted orbital with respect to the incident beam. Thus, in this work, we will consider only the case where the two target electrons are ejected from the same orbital-referred to as $(1t_{2x})^{-2}$, $(1t_{2y})^{-2}$, $(1t_{2z})^{-2}$, and $(2a_1)^{-2}$ whose double ionization energy are 40.5 eV (for the first three degenerated orbitals) and 60.9 eV [27] (for the $2a_1$ orbital), respectively. Under these conditions, we successively report in the following the evolution of the total cross sections, for the four subshells of the methane molecule, versus the β angle, the latter have been normalized to their $\beta = 0$ value (i.e. for a parallel orientation).

Let us first consider the $1t_{2x}$ molecular orbital, mainly governed by a $2p_{+1}$ orbital and then corresponding, in the present molecular description based on *real solid harmonics*, to an orbital collinear to the x molecular axis. This orbital type will be denoted P_X in the following.

Thus, applying the $R_y\ (0,\beta,0)$ rotation on the $1t_{2x}$ orbital means going from an initial configuration where the orbital is aligned with the x axis to a final configuration (denoted P_Z in the following) where the orbital is parallel to the z axis, as shown in equation (27) where the $R_y(0,\beta,0)$ transformations are summarized

$$R_y(0,\pi/2,0)\ :\ \begin{cases} P_X \rightarrow P_Z \\ P_Y \rightarrow P_Y \\ P_Z \rightarrow P_X. \end{cases} \tag{27}$$

In the left panel of Figure 2, we report the calculated total ionization cross sections for the $1t_{2x}$ orbital. The evident influence of the orbital alignment on the ionization process may be observed, in particular, in magnitude. Indeed, it clearly appears that at low collision energies ($E_i < 200$ eV) the total DI cross sections exhibit a maximum when the impacted orbital is collinear to the beam axis (the z axis), namely, for $\beta = \pi/2$ whereas for incident energies above 200 eV ($E_i > 200$ eV), the maximum of total DI cross sections is observed for $\beta = 0$ for a target orbital perpendicular to the beam axis. This previously reported behavior can be easily interpreted by geometrical considerations. Indeed, at low energies, the incident electron is sensitive to the orientation of the impacted orbital and the double ionization process is privileged when the orbital is aligned with the incident electron momentum revealing then a direct reflection of the anisotropic distributions of the electron density of the impacted molecular orbital. On the contrary, as the electron energy increases, the double ionization process is dominant when the target orbital is perpendicular to the incident beam (i.e. when the geometrical cross section is the highest) that meets the observations already made by Champion and Rivarola [28] who reported an increase of the total ionization cross sections in perpendicular configurations for electron-induced ionization of oriented water molecules. This particular feature is clearly highlighted in Figure 2 (right panel) where the variation of the $\sigma(0,\beta,0)/\sigma(0,0,0)$ ratio versus the β-angle is reported for various incident energies

Considering now the $1t_{2z}$ orbital (see Fig. 3) whose major component is $2p_0$, i.e. a P_Z orbital-type, we observe the opposite trend. Indeed, following the $R_y(0,\,\pi/2,0)$ rotation reported in equation (27) according to which a P_Z orbital becomes a P_X one, the $1t_{2z}$ orbital-initially aligned with the incident electron beam-becomes now perpendicular to the incident direction $(\alpha,\,\beta,\,\gamma\,) = (0,\,\pi/2,0)$. In these conditions, the $1t_{2z}$ orbital, initially aligned with the incident electron beam, now becomes perpendicular to the incident electron momentum ($\beta = \pi/2$), that leads to total cross sections whose maxima are located at ($\beta = 0$) for an orbital orientation parallel to the incident beam at low collision energies ($E_i <$ 200 eV) whereas when the incident energies exceeds 200 eV the cross sections are dominated for perpendicular alignment to the incident beam ($\beta = \pi/2$).

In Figure 4a, we report the result obtained for the $1t_{2y}$ molecular orbital mainly governed by a $2p_{-1}$ orbital and therefore denoted P_Y. In this case, it is clear that the rotation $R_y(0,\beta,0)$ will not change the orientation of the molecular orbital, which then remains aligned with the y axis (see Eq. (27)). A similar observation has also been performed for the $2a_1$ molecular state mainly governed by a spherical symmetry $2s$ component. Therefore, the results of total double ionization cross sections show an evident isotropy versus the molecular orientation (see Fig. 4b).

In Figure 5, the energy distributions of the secondary electrons ejected by double ionization of $1t_{2x}$ orbital oriented in the (0,0,0) and $(0,\,\pi/2,0)$ directions are shown. The obtained results clearly show that the DDCS are more affected by the target orientation at 100 eV than at 500 eV. Thus, in Figures 5a and 5b, we observe

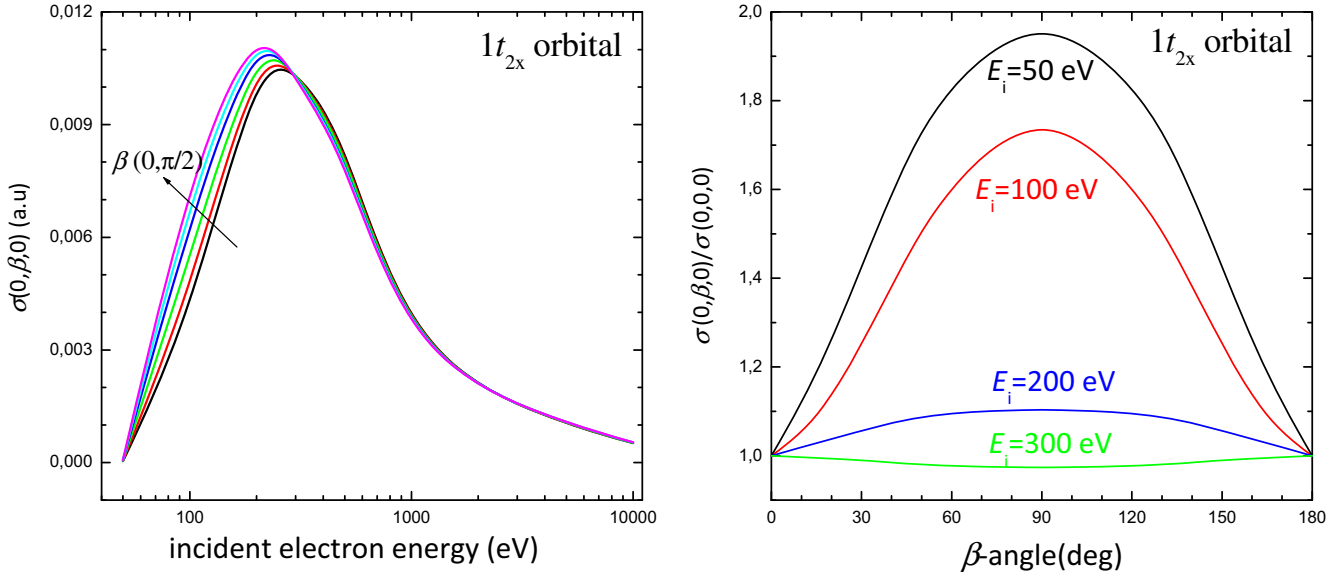

Fig. 2. Left panel: total double ionization cross sections (in atomic units) of the $1t_{2x}$ molecular orbital for particular orientations defined by the β-angle ranging from 0 to π. Right panel: variation of the total double ionization cross sections of the $1t_{2x}$ molecular orbital with the β-angle for several incident energies. Curves are normalized at β =0.

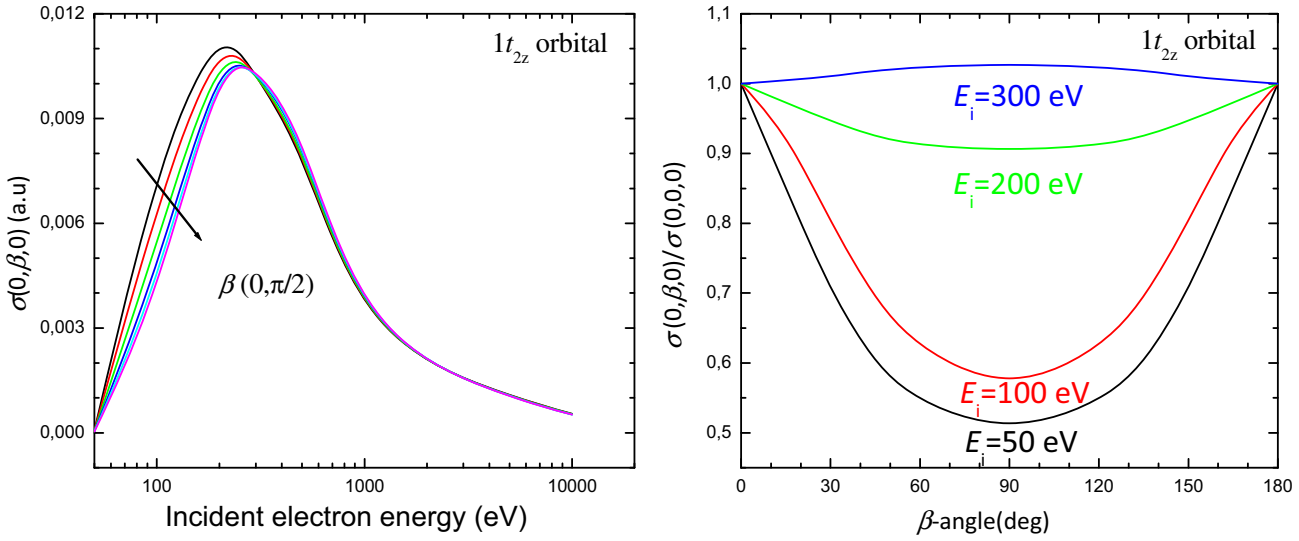

Fig. 3. Left panel: total double ionization cross sections of the $1t_{2z}$ molecular orbital for particular orientations defined by the β-angle ranging from 0 to π. Right panel: variation of the total double ionization cross sections of the $1t_{2z}$ molecular orbital with the β-angle for several incident energies. Curves are normalized at $\beta = 0$.

more pronounced energy distributions with a maximum of about 0.11 a.u. in the (0,0,0) direction versus about 0.14 a.u. in the (0, π/2,0) direction. On the contrary, when the incident electron energy increases, this anisotropy is less evident such as reported in Figures 5c and 5d where the energy distribution after a 500 eV electron-induced double ionization is reported for the (0,0,0) and the (0, π/2,0) direction, respectively. Let us note that similar observations were previously reported in reference [20] for oriented water molecules impacted by 100 eV electrons. More precisely, we found a doubly differential cross section of about 5.58 a.u. at $\beta =$ 0 (vs. 0.45 a.u. here) and of about 4.64 a.u. at $\beta = \pi/2$ (vs. 0.45 a.u. here, see Fig. 6).

In Figure 6, we report the evolution of the *global* energy distributions of the secondary electrons ejected by double ionization of a methane molecule oriented in the (0,0,0) and (0, π/2,0) directions, the latter being obtained by summing up all the molecular-state contributions. Whatever the incident energy, the DDCS are not sensitive to the molecular orientation. This result is probably due to the fact that when applying rotations, the molecular subshells interchange their contributions. This may

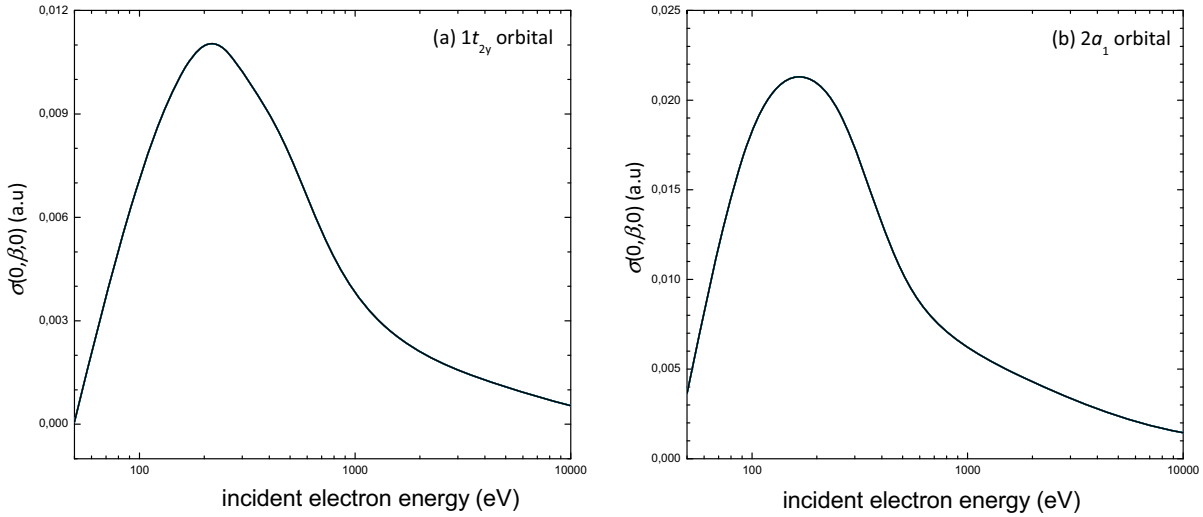

Fig. 4. Total double ionization cross sections for particular orientations defined by the β-angle ranging from 0 to π: (a) $1t_{2y}$ molecular orbital and (b) $2a_1$ molecular orbital.

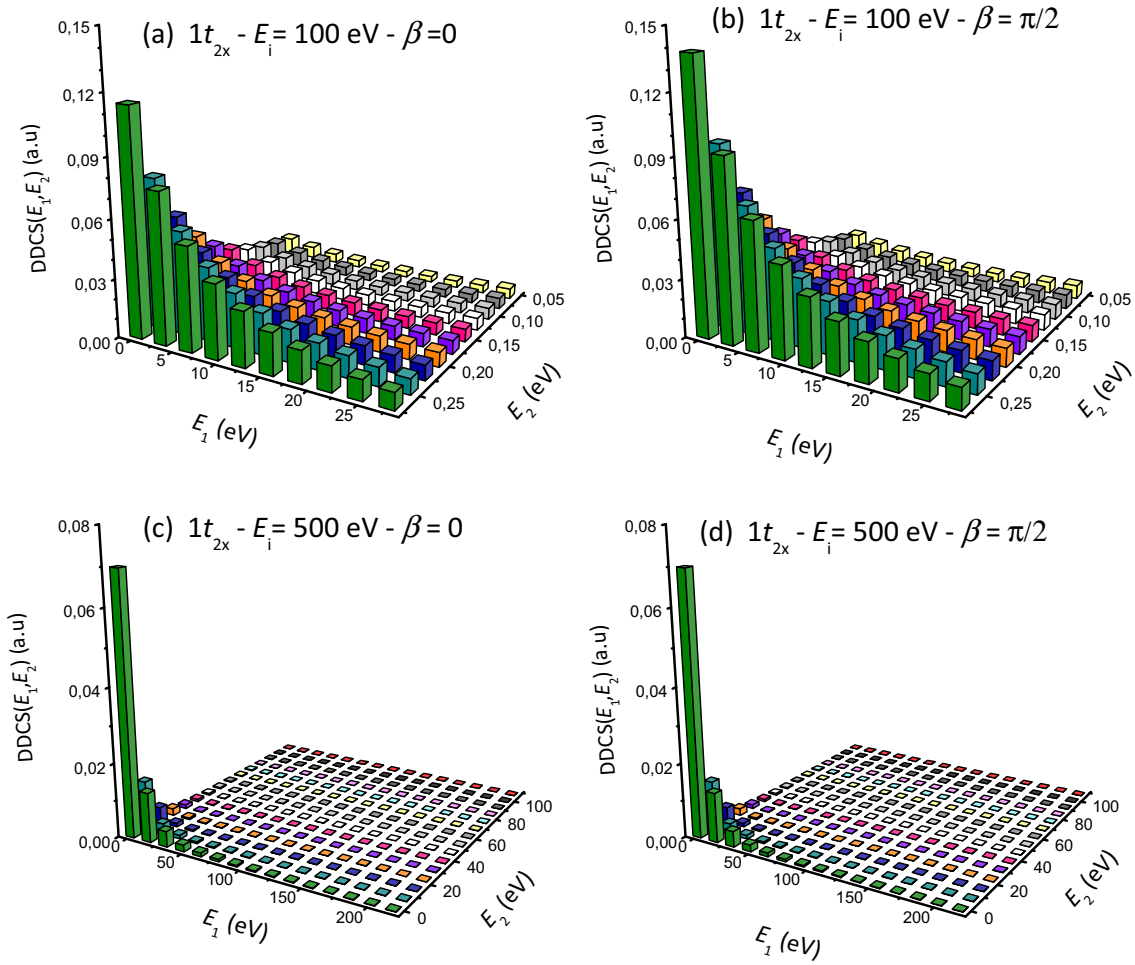

Fig. 5. Energetic distributions for the double ionization of the $1t_{2x}$ oriented orbital: (a) $(E_i, \beta) = (100\text{ eV}, 0)$, (b) $(E_i, \beta) = (100\text{ eV}, \pi/2)$, (c) $(E_i, \beta) = (500\text{ eV}, 0)$ and (d) $(E_i, \beta) = (500\text{ eV}, \pi/2)$.

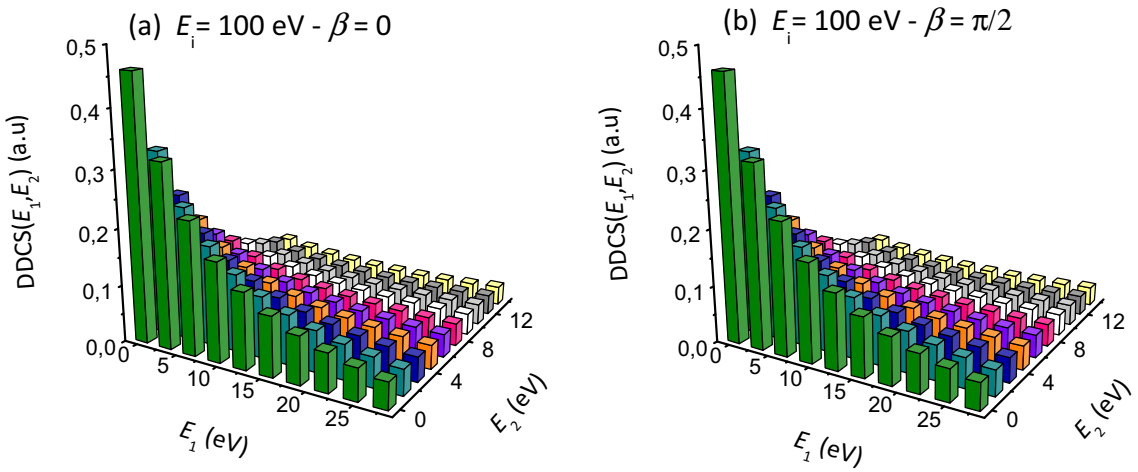

Fig. 6. Energetic distributions for the double ionization of methane molecule: (a) $(E_i,\ \beta) = (100\ \text{eV},0)$ and (b) $(E_i, \beta) = (100\ \text{eV}, \pi/2)$.

be attributed to the high symmetry of the methane molecule that may be considered as quasi-spherical.

4 Conclusions

In this paper we report the total cross sections studies for double ionization of oriented methane molecule. The calculations are here provided within the 1st Born approach for the case where the two target electrons are ejected from the same orbital referred to as $(1t_{2x})^{-2}$, $(1t_{2y})^{-2}$, $(1t_{2z})^{-2}$ and $(2a_1)^{-2}$. We clearly pointed a strong dependency of the double ionization process versus the molecule orientation in particular when the description is given *orbital by orbital*. On the contrary, when *global* total and double differential cross sections were considered, namely, by summing up all the subshell contributions, the double ionization exhibits an evident anisotropy attributed to the high symmetry of the methane molecule.

Besides, at low collision energies ($E_i < 200$ eV) we have shown that the ionization process was privileged for impacted orbitals aligned with the incident electron momentum indicating a direct signature of the anisotropic distributions of the electron density of the impacted orbitals, this effect being inverted for increasing projectile energies.

Finally, let us remind that differences between first- and second-order Born approximations may be very important as for H_2O where 2nd Born predictions highlighted noticeable cross sections in specific geometrical configurations where first-order predictions were negligible. Such observations have not been reported here for the CH_4 molecule that has undoubtedly to be confirmed by higher-order calculations as well as further experiments.

Author contribution statement

All authors participated in the numerical developments Monte Carlo simulation development as well as the writing and the revising of the text.

References

1. E.W. McDaniel, J.B.A. Mitchell, M.E. Rudd, *Atomic Collision* (Wiley, New York, 1993)
2. C.S. Enos, A.R. Lee, and A.G. Brenton, Int. J. Mass Spectrom. Ion Process. **104**, 137 (1991)
3. K. Mitsuke, T. Takami, K. Ohno, J. Chem. Phys. **91**, 1618 (1989)
4. D.H. Katayama, R.E. Huffman, C.L. O'Bryan, J. Chem. Phys. **59**, 4309 (1973)
5. K. Tachibana, M. Nishida, H. Harima, Y. Urano, J. Phys. D: Appl. Phys. **17**, 1727 (1984)
6. R. Zellner, G. Weibring, Z. Phys. Chem. **161**, 167 (1989)
7. A.O. Nier, Int. J. Mass Spectrom. Ion Phys. **66,** 55 (1985)
8. S.P. Khare, M.K. Sharma, S. Tomar, J. Phys. B: At. Mol. Opt. Phys. **32**, 3147 (1999)
9. O. Chuluunbaatar, B. Joulakian, I.V. Puzynin, K.H. Tsookhuu, S.I. Vinitsky, J. Phys. B **41**, 015204 (2008)
10. A. Mansouri, C. Dal Cappello, S. Houamer, I. Charpentier, A. Lahmam-Bennani, J. Phys. B: At. Mol. Opt. Phys. **37**, 1203 (2004)
11. A. Lahmam-Bennani, A. Duguet, S. Roussin, J. Phys. B **35**, L59 (2002)
12. C. Li, A. Lahmam-Bennani, E.M. Staicu Casagrande, C. Dal Cappello, J. Phys. B: At. Mol. Opt. Phys. **44**, 115201 (2011)
13. E.M. Staicu Casagrande, C. Li, A. Lahmam-Bennani, C. Dal Cappello, M. Schulz, M. Ciappina, J. Phys. B: At. Mol. Opt. Phys. **44**, 055201 (2011)
14. E.M. Staicu Casagrande, C. Li, A. Lahmam-Bennani, C. Dal Cappello, J. Phys. B: At. Mol. Opt. Phys. **47,** 115203 (2014)
15. Th. Weber, A. Czasch, O. Jagutzki, A. Müller, V. Mergel, A. Kheifets, J. Feagin, E. Rotenberg, G. Meigs, M.H. Prior, S. Daveau, A.L. Landers, C.L. Cocke, T. Osipov, H. Schmidt- Böcking, R. Dörner, Phys. Rev. Lett. **92**, 163001 (2004)
16. M. Gisselbrecht, M. Lavollée, A. Huetz, P. Bolognesi, L. Avaldi, D.P. Seccombe, T.J. Reddish, Phys. Rev. Lett. **96**, 153002 (2006)
17. C. Champion, D. Oubaziz, H. Aouchiche, Yu.V. Popov, C. Dal Cappello, Phys. Rev. A **81**, 032704 (2010)

18. D. Oubaziz, H. Aouchiche, C. Champion, Phys. Rev. A **83**, 012708 (2011)
19. Z. Aitelhadjali, S. Kessal, M.A. Quinto, D. Oubaziz C. Champion, Int. J. Mass Spectrom. **403**, 53 (2016)
20. D. Oubaziz, C. Champion, H. Aouchiche, Phys. Rev. A **88**, 042709 (2013)
21. I.A. Ivanov, A.S. Kheifets, Phys. Rev. A **85**, 013406 (2012)
22. W. Vanroose, F. Martin, T.N. Rescigno, C.W. McCurdy, Phys. Rev. A **70**, 050703 (2004)
23. R. Moccia, J. Chem. Phys. **40**, 2164 (1964)
24. P. Defrance, T.M. Kereselidze, I.L. Noselidze, M.F. Tzulukidze, J. Phys. B: At. Mol. Opt. Phys. **34**, 4957 (2001)
25. P. Defrance, J.J. Jureta, T. Kereselidze, J. Lecointre, Z.S. Machavariani, J. Phys. B: At. Mol. Opt. Phys. **42**, 025202 (2009)
26. E. Bahati, H. Cherkani-Hassani, P. Defrance, J.J. Jureta, T. Kereselidze, Z. Machavariani, I. Noselidze, J. Phys. B: At. Mol. Opt. Phys. **38**, 1261 (2005)
27. W.J. Griffiths, S. Svensson, A. Naves de Brito, N. Correia, M.L. Langfords, F.M. Harris, Rapid Commun. Mass Spectrom. **6**, 438 (1992)
28. C. Champion, R.D. Rivarola, Phys. Rev. A **82**, 042704 (2010)